Volume 55 | Number 33 | 28 April 2019 | Pages 4741–4890

ChemComm

Chemical Communications

rsc.li/chemcomm

ISSN 1359-7345

ROYAL SOCIETY OF CHEMISTRY | Celebrating IYPT 2019

COMMUNICATION

Kyu Tae Lee, Taeghwan Hyeon *et al.*

Synthesis of nanostructured P2-$Na_{2/3}MnO_2$ for high performance sodium-ion batteries

ChemComm

COMMUNICATION

View Article Online
View Journal | View Issue

Cite this: *Chem. Commun.*, 2019, 55, 4757

Received 12th February 2019,
Accepted 7th March 2019

DOI: 10.1039/c9cc01215j

rsc.li/chemcomm

Synthesis of nanostructured P2-$Na_{2/3}MnO_2$ for high performance sodium-ion batteries†

Euiyeon Jung, ‡[ab] Yuwon Park, ‡[b] Kunsu Park,‡[ab] Mi-Sook Kwon,[b] Mihyun Park,[ab] Arun Kumar Sinha,[ab] Byoung-Hoon Lee,[ab] Jiheon Kim, [ab] Hyeon Seok Lee,[ab] Sue In Chae,[ab] Sung-Pyo Cho,[c] Kyu Tae Lee *[b] and Taeghwan Hyeon *[ab]

We report a facile two-step method to synthesize nanostructured P2-$Na_{2/3}MnO_2$ *via* ligand exchange and intercalation of sodium ions into ultrathin manganese oxide nanoplates. Sodium storage performance of the synthesized material shows a high capacity (170 mA h g^{-1}) and an excellent rate performance.

Lithium ion batteries have been the predominant choice of energy storage systems for portable devices and electronic vehicles in the last few decades due to their high energy density and long cycle life.[1–3] As a new class of green energy storage and conversion system, sodium ion batteries (SIBs) have received much attention owing to the high natural abundance and low cost of sodium resources.[4–6] Sodium has a redox potential (−2.71 V *vs.* SHE) close to that of lithium (−3.04 V *vs.* SHE) which makes it an attractive alternative to lithium ion batteries.[7] However, there are still challenges remaining for sodium-ion batteries. One critical issue is finding cathode materials with high reversible capacity and good cycle life to meet the performance expectation for electronic devices.[8] For this reason, many different types of oxide materials including spinel oxides,[9] tunnel-structured oxides,[10,11] and layered transition metal oxides, have been explored for the last few years. Among them, layered sodium transition metal oxides (Na_xMO_2, M = Mn, Ni, Co, Fe, *etc.*, $x < 1$) are the most studied cathode materials due to their high energy density.[12–15]

Sodium manganese oxide (NMO) is a promising cathode material because of its high availability and low cost, making it suitable for large-scale batteries. Sodium manganese oxides are known to deliver large reversible capacities. Caballero *et al.* reported that P2-type layered $Na_{2/3}MnO_2$ (P2-NMO) can deliver a large initial capacity of 160 mA h g^{-1}.[16] However, many research groups reported problems with P2-NMO such as poor rate capability and cycle retention.[17–19]

Nanostructured materials have received a lot of attention as a solution to such problem by enhancing ion kinetics.[20–22] Herein, we report a facile and unique synthetic method to produce a nanostructured P2-$Na_{2/3}MnO_2$ cathode material *via* a two-step method, starting from ultrathin manganese oxide nanoplates. Nanostructured P2-$Na_{2/3}MnO_2$ exhibited remarkable sodium storage performance, such as a high reversible capacity of 170 mA h g^{-1}, excellent rate performance delivering 135 mA h g^{-1} at 10C rate, and negligible capacity fading over 50 cycles. The improved electrochemical performance is attributable to grain boundaries between the nanostructured domains that are embedded inside the crystals. Our facile synthetic method could be generalized to other sodium metal oxide systems for the design of nanostructured cathodes for high performance SIBs.

Nanostructured P2-$Na_{2/3}MnO_2$ is synthesized by the two-step method as described in Fig. 1. Firstly, ultrathin manganese oxide nanoplates were synthesized following the previously reported method.[23] The as-synthesized brownish nanoplates are 8 nm long and less than 1 nm thick, assembled into a lamellar structure (Fig. 2a and b). For the ligand exchange reaction, the prepared manganese oxide nanoplates were dispersed in tetrahydrofuran (THF) and mixed with 1 M sodium hydroxide (NaOH)–ethylene glycol solution. The mixed solution was stirred at 65 °C for 48 hours and during this ligand exchange reaction, the hydrophobic, 2,3-dihydroxynaphthalene (2,3-DHN) organic surfactant was replaced by the hydroxide ions causing the delamination of the lamellar structure of the nanoplates.[23,24] The surface charge was neutralized by the sodium ions on the surface of the nanoplates.[25] This process destroyed the π–π interactions between the 2,3-DHN molecules to produce discrete Na^+-adsorbed manganese oxide nanoplates. After the heat treatment at 500 °C in air, Na^+-adsorbed nanoplates were turned into layered sodium manganese oxide nanoparticles (20–50 nm) (Fig. 2c). From the energy dispersive X-ray spectroscopy (EDS) and high-resolution transmission electron microscopy (HRTEM) images (Fig. 2c and d), we observed sodium manganese oxide nanoparticles (NMO NPs)

[a] *Center for Nanoparticle Research, Institute for Basic Science (IBS), Seoul 08826, Korea*
[b] *School of Chemical and Biological Engineering, Seoul National University, Seoul 08826, Korea. E-mail: ktlee@snu.ac.kr, thyeon@snu.ac.kr*
[c] *National Center for Inter-university Research Facilities, Seoul National University, Seoul 08826, Korea*

† Electronic supplementary information (ESI) available. See DOI: 10.1039/c9cc01215j
‡ These authors contributed equally to this work.

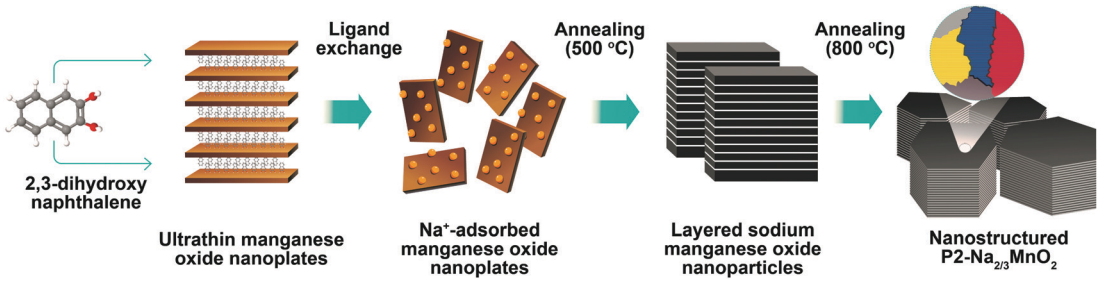

Fig. 1 Schematic illustration of the two-step method to synthesize nanostructured P2-$Na_{2/3}MnO_2$.

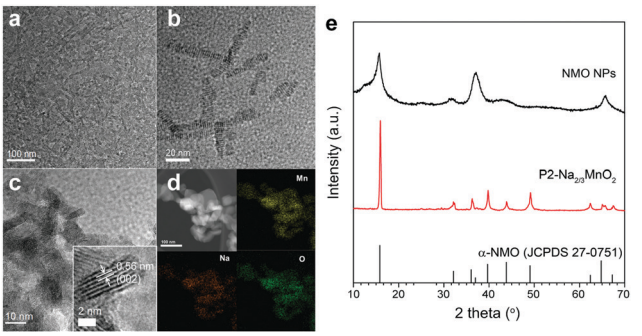

Fig. 2 (a) and (b) TEM images of manganese oxide nanoplates, (c) TEM image, (d) STEM image and EDS images of NMO NPs and (e) XRD patterns of NMO NPs and nanostructured P2-$Na_{2/3}MnO_2$.

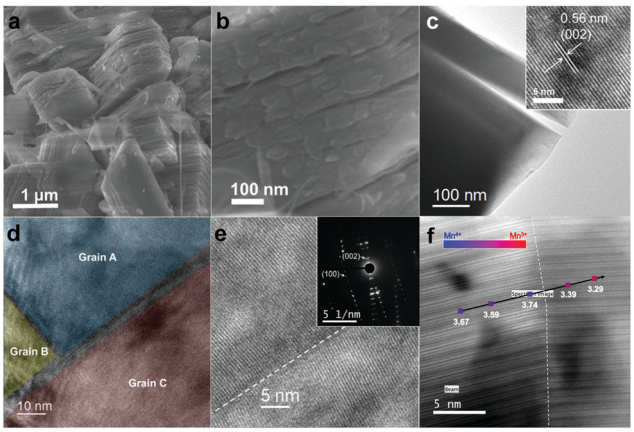

Fig. 3 (a) and (b) SEM images and (c) TEM image of the nanostructured P2-$Na_{2/3}MnO_2$ (Inset: Magnified HRTEM image). HRTEM images of (d) three neighboring grains: A, B, and C (e) the interface region with a SAED pattern (inset) indicating the different orientations. (f) High-angle annular dark-field STEM image of the interface region with an EELS line scan.

with a lattice spacing of ~0.56 nm, similar to the *d*-spacing of a (002) plane in P2-hexagonal phase. In contrast, we obtained micrometer-sized Mn_2O_3 particles under the same annealing condition without the NaOH treatment, indicating that the ligand exchange step not only supplies Na^+ ions but also restricts the particle growth (Fig. S1, ESI†).[26–28] The XRD spectrum of the NMO NPs shows broad peaks (00*l*), indicating that the particles are stacked in a turbostratic manner without sufficient crystallinity causing poor reversible sodium storage (Fig. 2e and Fig. S2, ESI†). We performed further annealing at 800 °C to acquire a well-crystallized P2-$Na_{2/3}MnO_2$ which is well indexed to a hexagonal structure with a space group of *P*63/*mmc* ($Na_{0.7}MnO_{2.05}$, JCPDS 27-0751) known as the α phase of NMO (Fig. 2e). Additional heat treatment at 800 °C triggered the assembly of the NMO nanoparticles and caused a significant increase in size. The SEM images (Fig. 3a and b) show tens of micrometer-sized plates stacked in an orderly manner and the TEM image (Fig. 3c) demonstrates the highly crystalline nature of the P2-type structure.

The cross-sectional specimens of P2-$Na_{2/3}MnO_2$ was obtained using a focused ion beam (FIB) and analyzed by spherical aberration-corrected scanning transmission electron microscopy (Cs-STEM) combined with electron energy loss spectroscopy (EELS). The HRTEM image shows nanoscale domains inside the crystal which are clearly separated by grain boundaries (Fig. 3d). The selective area electron diffraction pattern (SAED) near the grain boundary reveals that all the grains have the P2-type structure despite their different orientations (inset of Fig. 3e). From the EELS line scan across the grain boundary, we calculated the integrated Mn L_3/L_2 white line ratios (Fig. 3f).[29,30] More details on the method of calculating the Mn L_3/L_2 ratio can be found in Fig. S3 (ESI†). It is well known that the oxidation state of transition metals can be derived from the white line intensity ratio (Fig. S3, ESI†).[29–31] The calculated Mn L_3/L_2 ratios and the corresponding Mn oxidation state values are listed in Table S1 (ESI†). We observed a change in the average Mn oxidation state from 3.74 to 3.29 across the grain boundary, which indicates that the adjacent domains have different oxidation states as indicated in Fig. 3f. There are known to be two polymorphs in $Na_{0.7}MnO_2$: α-$Na_{0.7}MnO_{2+z}$ ($0.05 \leq z \leq 0.25$) with an average Mn oxidation state of 3.8 and β-$Na_{0.7}MnO_{2+z}$ ($z < 0.05$) with an average Mn oxidation state of 3.3 (Fig. S4, ESI†).[32] The characteristics of crystal structures and the average Mn oxidation states depend on the method of cooling during the synthesis. α-$Na_{0.7}MnO_{2+z}$ ($0.05 \leq z \leq 0.25$) and β-$Na_{0.7}MnO_{2+z}$ ($z < 0.05$) are obtained through a conventional cooling and quenching, respectively. However, we obtained a nanoscale mixture of NMO comprising two different phases through our unique approach of synthesizing nanostructured P2-NMO.

The composite behavior of nanostructured P2-NMO was also supported by the differential capacity plot (d*Q*/d*V*) (Fig. 4a). The d*Q*/d*V* of nanostructured P2-NMO displays both characteristic peaks of the α-NMO and β-NMO phases. The d*Q*/d*V* peaks below 2.27 V indicate redox peaks of α-NMO (Fig. 4a, asterisk signs),

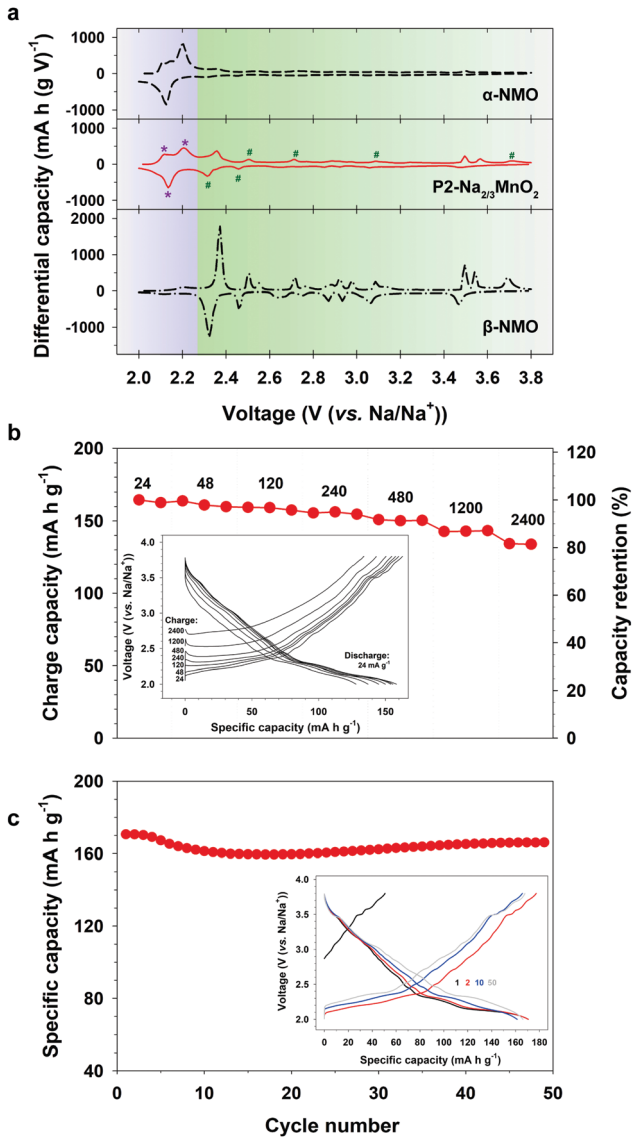

Fig. 4 Sodium storage performance of the nanostructured P2-$Na_{2/3}MnO_2$. (a) Differential capacity plots at 12 mA g^{-1}. Data for α-NMO and β-NMO were adapted from ref. 32. (b) Rate performance at various charge current densities. (c) Cycling performance at 12 mA g^{-1} (inset: corresponding voltage profiles).

whereas the peaks above 2.27 V correspond to those of β-NMO (Fig. 4a, number signs). Redox peaks corresponding to the α phase are much stronger than those corresponding to the β phase. This implies that the majority of grains is in α phase, which is consistent with the XRD pattern of the nanostructured P2-NMO.

Nanostructured P2-$Na_{2/3}MnO_2$ was examined as a cathode material for sodium ion batteries. Firstly, we evaluated rate performance at various charging rates from 24 to 2400 mA g^{-1} (0.1–10C rate) as shown in Fig. 4b. The cell was discharged at a fixed rate of 24 mA g^{-1}. P2-$Na_{2/3}MnO_2$ showed excellent rate performance, such as 135 mA h g^{-1} at 10C rate, which corresponds to 80% of the reversible capacity delivered at 0.1C rate. It has been shown that the lithium diffusion coefficient along the grain boundaries is three orders of magnitude higher than that across the grain boundaries due to the much lower activation energy.[33,34] Therefore, we suggest that the improved rate performance of nanostructured P2-NMO is due to the nanoscale domains of P2-NMO. Nanostructured grain boundaries (Fig. S5, ESI†) facilitated the solid state diffusion of Na^+ ions through a bulk particle, resulting in the excellent rate capability (Fig. 4b). Moreover, the cycle performance and the corresponding charge–discharge profiles were taken at a current density of 12 mA g^{-1} in the voltage range of 2.0–3.8 V (Fig. 4c). The nanostructured P2-NMO electrode delivered a high initial capacity of 170 mA h g^{-1} with negligible capacity fading over 50 cycles, outperforming the recently reported sodium manganese oxide electrodes (Table S2, ESI†).

In summary, nanostructured P2-$Na_{2/3}MnO_2$ has been prepared *via* ligand exchange and crystallization of ultrathin manganese oxide nanoplates. Through this novel scheme of design, we produced well-crystallized P2-NMO bulk particles comprising nanoscale domains. As a cathode for Na-ion batteries, it showed excellent electrochemical performance including a high specific capacity of 170 mA h g^{-1} and excellent rate performance. Our unique two-step strategy of fabricating nanostructured sodium metal oxide materials will pave a new way for the design and synthesis of electrodes for high-performance rechargeable batteries.

This work was supported by Institute for Basic Science (IBS-R006-D1) and the National Research Foundation of Korea (NRF) Grant (NRF-2018R1A5A1024127).

Conflicts of interest

There are no conflicts to declare.

Notes and references

1 M. S. Whittingham, *Chem. Rev.*, 2014, **114**, 11414.
2 J. B. Goodenough, *Energy Storage Mater.*, 2015, **1**, 158.
3 M. Armand and J.-M. Tarascon, *Nature*, 2008, **451**, 652.
4 W. Luo, F. Shen, C. Bommier, H. Zhu, X. Ji and L. Hu, *Acc. Chem. Res.*, 2016, **49**, 231.
5 H. Kim, D. J. Kim, D.-H. Seo, M. S. Yeom, K. Kang, D. K. Kim and Y. Jung, *Chem. Mater.*, 2012, **24**, 1205.
6 S.-W. Kim, D.-H. Seo, X. Ma, G. Ceder and K. Kang, *Adv. Energy Mater.*, 2012, **2**, 710.
7 S. P. Ong, V. L. Chevrier, G. Hautier, A. Jain, C. Moore, S. Kim, X. Ma and G. Ceder, *Energy Environ. Sci.*, 2011, **4**, 3680.
8 N. Yabuuchi, K. Kubota, M. Dahbi and S. Komaba, *Chem. Rev.*, 2014, **114**, 11636.
9 X. Liu, X. Wang, A. Iyo, H. Yu, D. Li and H. Zhou, *J. Mater. Chem. A*, 2014, **2**, 14822.
10 Y. Cao, L. Xiao, W. Wang, D. Choi, Z. Nie, J. Yu, L. V. Saraf, Z. Yang and J. Liu, *Adv. Mater.*, 2011, **23**, 3155.
11 J.-Y. Li, X.-L. Wu, X.-H. Zhang, H.-Y. Lu, G. Wang, J.-Z. Guo, F. Wan and R.-S. Wang, *Chem. Commun.*, 2015, **51**, 14848.
12 M. H. Han, E. Gonzalo, G. Singh and T. Rojo, *Energy Environ. Sci.*, 2015, **8**, 81.
13 N. Yabuuchi, M. Kajiyama, J. Iwatate, H. Nishikawa, S. Hitomi, R. Okuyama, R. Usui, Y. Yamada and S. Komaba, *Nat. Mater.*, 2012, **11**, 512.
14 D. Yuan, W. He, F. Pei, F. Wu, Y. Wu, J. Qian, Y. Cao, X. Ai and H. Yang, *J. Mater. Chem. A*, 2013, **1**, 3895.
15 D. Kim, S.-H. Kang, M. Slater, S. Rood, J. T. Vaughey, N. Karan, M. Balasubramanian and C. S. Johnson, *Adv. Energy Mater.*, 2011, **1**, 333.

16 A. Caballero, L. Hernan, J. Morales, L. Sanchez, J. S. Pena and M. A. G. Aranda, *J. Mater. Chem.*, 2002, **12**, 1142.
17 N. Bucher, S. Hartung, A. Nagasubramanian, Y. L. Cheah, H. E. Hoster and S. Madhavi, *ACS Appl. Mater. Interfaces*, 2014, **6**, 8059.
18 D. Su, C. Wang, H.-J. Ahn and G. Wang, *Chem. – Eur. J.*, 2013, **19**, 10884.
19 T.-R. Chen, Z.-G. Wu, W. Xiang, E.-H. Wang, C.-J. Wu, M.-Z. Chen, X.-D. Guo and B.-H. Zhong, *Ceram. Int.*, 2017, **43**, 6303.
20 M. F. Oszajca, M. I. Bodnarchuk and M. V. Kovalenko, *Chem. Mater.*, 2014, **26**, 5422.
21 V. Raju, J. Rains, C. Gates, W. Luo, X. Wang, W. F. Stickle, G. D. Stucky and X. Ji, *Nano Lett.*, 2014, **14**, 4119.
22 E. Kang, Y. S. Jung, A. S. Cavanagh, G.-H. Kim, S. M. George, A. C. Dillon, J. K. Kim and J. Lee, *Adv. Funct. Mater.*, 2011, **21**, 2430.
23 M. Park, N. Lee, S. H. Choi, K. An, S.-H. Yu, J. H. Kim, S.-H. Kwon, D. Kim, H. Kim, S.-I. Baek, T.-Y. Ahn, O. K. Park, J. S. Son, Y.-E. Sung, Y.-W. Kim, Z. Wang, N. Pinna and T. Hyeon, *Chem. Mater.*, 2011, **23**, 3318.
24 R. Ma, Z. Liu, L. Li, N. Iyi and T. Sasaki, *J. Mater. Chem.*, 2006, **16**, 3809.
25 S.-H. Yu, M. Park, H. S. Kim, A. Jin, M. Shokouhimehr, T.-Y. Ahn, Y.-W. Kim, T. Hyeon and Y.-E. Sung, *RSC Adv.*, 2014, **4**, 12087.
26 Y. Piao, H. S. Kim, Y.-E. Sung and T. Hyeon, *Chem. Commun.*, 2010, **46**, 118.
27 Y. Piao, J. Kim, H. B. Na, D. Kim, J. S. Baek, M. K. Ko, J. H. Lee, M. Shokouhimehr and T. Hyeon, *Nat. Mater.*, 2008, **7**, 242.
28 Z. Yang, J. Shen, N. Jayaprakash and L. A. Archer, *Energy Environ. Sci.*, 2012, **5**, 7025.
29 D. H. Pearson, B. Fultz and C. C. Ahn, *Appl. Phys. Lett.*, 1988, **53**, 1405.
30 D. H. Pearson, C. C. Ahn and B. Fultz, *Phys. Phys. Rev. B*, 1993, **47**, 8471.
31 H. K. Schmid and W. Mader, *Micron*, 2006, **37**, 426.
32 M.-S. Kwon, S. G. Lim, Y. Park, S.-M. Lee, K. Y. Chung, T. J. Shin and K. T. Lee, *ACS Appl. Mater. Interfaces*, 2017, **9**, 14758.
33 H. Moriwake, A. Kuwabara, C. A. J. Fisher, R. Huang, T. Hitosugi, Y. H. Ikuhara, H. Oki and Y. Ikuhara, *Adv. Mater.*, 2013, **25**, 618.
34 N. Balke, S. Jesse, A. N. Morozovska, E. Eliseev, D. W. Chung, Y. Kim, L. Adamczyk, R. E. Garcia, N. Dudney and S. V. Kalinin, *Nat. Nanotechnol.*, 2010, **5**, 749.

